JOURNAL OF COMPUTATIONAL PHYSICS 83, 148–184 (1989)

ENO Schemes with Subcell Resolution*

AMI HARTEN

School of Mathematical Sciences, Tel-Aviv University, Israel and
Department of Mathematics, University of California,
Los Angeles, California

Received July 9, 1987; revised February 29, 1988

DEDICATED TO EUGENE ISAACSON ON HIS 70TH BIRTHDAY

In this paper, we introduce the notion of subcell resolution, which is based on the observation that unlike point values, cell-averages of a discontinuous piecewise-smooth function contain information about the exact location of the discontinuity within the cell. Using this observation we design an essentially non-oscillatory (ENO) reconstruction technique which is exact for cell averages of discontinuous piecewise-polynomial functions of the appropriate degree. Later on we incorporate this new reconstruction technique into Godunov-type schemes in order to produce a modification of the ENO schemes which prevents the smearing of contact discontinuities.

1. INTRODUCTION

In [6–8] we have introduced a class of essentially nonoscillatory (ENO) schemes that generalizes Godunov's scheme [2] to a high order of accuracy.

In this paper we present a modification of the ENO schemes which is designed to prevent smearing of linear discontinuities. This is done by adding a correction term to the numerical flux of the ENO scheme. First, we shall derive a correction term to account for discontinuities in the scalar constant coefficient case. Later we shall apply the scalar correction to the linearly degenerate characteristic field in the Euler equations in order to improve the resolution of contact discontinuities.

Let $\{I_j \times [t_n, t_{n+1})\}$, where $I_j = [x_{j-1/2}, x_{j+1/2}]$, $x_\alpha = \alpha h$, $t_k = k\tau$, be a partition of $\mathbf{R} \times \mathbf{R}^+$. Let $\bar{u}_j^n$ be the "cell-average" of u at time t_n, i.e.,

$$\bar{u}_j^n = \frac{1}{h} \int_{I_j} u(x, t_n)\, dx. \tag{1.1}$$

* Research was supported under NSF Grant DMS85-03294, DARPA Grant in the ACMP Program, ONR Grant N00014-86-K-0691, NASA Ames Interchange NCA2-185, and NASA Langley Grant NAG1-270. Also research was partially supported under the National Aeronautics and Space Administration under NASA Contract NAS1-18107 while the author was in residence at the Institute for Computer Applications in Science and Engineering (ICASE), NASA Langley Research Center, Hampton, VA 23665-5225.

0021-9991/89 $3.00

The cell-average of the solution to the initial value problem

$$u_t + f(u)_x = 0, \qquad u(x, 0) = u_0(x) \tag{1.2}$$

satisfies

$$\bar{u}_j^{n+1} = \bar{u}_j^n - \lambda[\tilde{f}(x_{j+1/2}, t_n; u) - \tilde{f}(x_{j-1/2}, t_n; u)], \tag{1.3a}$$

where $\lambda = \tau/h$ and

$$\tilde{f}(x, t; u) = \frac{1}{\tau}\int_0^\tau f(u(x, t+\eta))\, d\eta. \tag{1.3b}$$

The ENO schemes can be written in the standard conservation form

$$v_j^{n+1} = v_j^n - \lambda(\hat{f}_{j+1/2} - \hat{f}_{j-1/2}) \equiv [\bar{E}_h(\tau)\cdot v^n]_j; \tag{1.4a}$$

here $\bar{E}_h$ denotes the numerical solution operator and $\hat{f}_{j+1/2}$, the numerical flux, denotes a function of $2k$ variables

$$\hat{f}_{j+1/2} = f(v_{j-k+1}^n, \ldots, v_{j+k}^n) \tag{1.4b}$$

which is consistent with the flux $f(u)$ in (1.2), in the sense that $\hat{f}(u, u, \ldots, u) = f(u)$. Unlike standard difference schemes, v_j^n in the ENO schemes is a high-order approximation to the cell-average $\bar{u}_j^n$, and not to the point value $u(x_j, t_n)$. Setting $v_j^n = \bar{u}_j^n$ in the numerical scheme (1.4) and comparing it to relation (1.3), we see that if the numerical flux $\hat{f}_{j+1/2} = \hat{f}(\bar{u}_{j-k+1}^n, \ldots, \bar{u}_{j+k}^n)$ can be expanded as

$$\hat{f}(\bar{u}_{j-k+1}^n, \ldots, \bar{u}_{j+k}^n) = \frac{1}{\tau}\int_0^\tau f(u(x_{j+1/2}, t_n + \eta))\, d\eta + d(x_{j+1/2})h^r + O(h^{r+1}) \tag{1.5a}$$

then the truncation error

$$\bar{u}_j^{n+1} - [\bar{E}_h \cdot \bar{u}^n]_j = \lambda[d(x_{j+1/2}) - d(x_{j-1/2})]h^r + O(h^{r+1}), \tag{1.5b}$$

is $O(h^{r+1})$ wherever $d(x)$ is Lipschitz continuous, i.e., the scheme (1.4) is rth order accurate in the sense of cell averages.

The most important ingredient in the ENO schemes is a preocedure to reconstruct a piecewise-smooth function $w(x)$ from its given cell-averages $\{\bar{w}_j\}$. This reconstruction, which we denote by $R(x; \bar{w})$, is a piecewise-polynomial function of x that has a uniform polynomial degree $(r-1)$ and satisfies:

(i) at all points x for which there is a neighborhood where w is smooth

$$R(x; \bar{w}) = w(x) + e(x)h^r + O(h^{r+1}); \tag{1.6a}$$

(ii) conservation in the sense of

$$\frac{1}{h}\int_{x_{j-1/2}}^{x_{j+1/2}} R(\xi; \bar{w})\, d\xi = \bar{w}_j; \tag{1.6b}$$

(iii) it is essentially non-oscillatory

$$\mathrm{TV}(R(\cdot; \bar{w})) \leqslant \mathrm{TV}(\bar{w}) + O(h^{1+P}), \qquad P > 0, \tag{1.6c}$$

where TV denotes total variation in x.

Using such a reconstruction (1.6) we can express the abstract form of the ENO schemes by

$$\bar{E}_h(\tau) \cdot \bar{w} = A(I) \cdot E(\tau) \cdot R(\cdot; \bar{w}). \tag{1.7a}$$

Here $A(I)$ is the cell-averaging operator

$$A(I) \cdot w = \frac{1}{|I|}\int_I w(y)\, dy \tag{1.7b}$$

and $E(t)$ is the exact evolution operator of the IVP (1.2), i.e.,

$$u(\cdot, t) = E(t)u_0. \tag{1.7c}$$

We note that (1.7a) with the piecewise constant reconstruction

$$R(x; \bar{w}) = \bar{w}_j \qquad \text{for} \quad x_{j-1/2} \leqslant x \leqslant x_{j+1/2} \tag{1.8}$$

is exactly the first-order accurate Godunov's scheme [1]; (1.7a) with the piecewise linear reconstruction

$$R(x; \bar{w}) = \bar{w}_j + S_j(x - x_j) \qquad \text{for} \quad x_{j-1/2} \leqslant x < x_{j+1/2}, \tag{1.9a}$$

where

$$S_j = w_x(x_j) + O(h), \tag{1.9b}$$

is the abstract form of the second-order accurate extensions to Godunov's scheme described in [6–8]. We shall refer to these schemes as MUSCL-type schemes due to their similarity to van Leer's work in [9].

In the first-order case (1.8), the scheme (1.7a) can be expressed in the conservation form (1.4) with the numerical flux

$$\tilde{f}_{j+1/2} = f^R(v_j^n, v_{j+1}^n); \tag{1.10}$$

here $f^R(u_1, u_2)$ is an approximation to the flux at the origin in a Riemann problem with u_1 to the left and u_2 to the right.

In the second-order case (1.9), the numerical flux of the abstract scheme cannot be expressed in a simple closed form, and we approximate it by

$$\tilde{f}_{j+1/2} = \tilde{f}^{\mathrm{ENO}}_{j+1/2} = f^R(v^L_{j+1/2}, v^R_{j+1/2}), \tag{1.11a}$$

where

$$v^L_{j+1/2} = v^n_j + h(1-\lambda a^n_j)S^n_j/2, \qquad v^R_{j+1/2} = v^n_{j+1} - h(1+\lambda a^n_{j+1})S^n_{j+1}/2; \tag{1.11b}$$

here $a^n_j = f'(v^n_j)$.

In this paper we pay special attention to the second-order accurate scheme (1.11), because at present this seems to be the state of the art. This class of second-order schemes (with various choices of S^n_j) performs rather well in smooth regions and shocks. However, it exhibits excessive smearing of linear discontinuities, i.e., contact discontinuitites. Usually such discontinuities are smeared more and more in time at the ate $O(n^{1/3})$, where n is the number of time-steps. To understand this smearing we note in (1.7) that whenever a discontinuity in the reconstruction R is propagated by the evolution operator E into the interior of the cell, then the cell-averaging operator $A(I)$ replaces this sharp discontinuity by a smeared transition. In the linear case there is nothing to stop this process and therefore it goes on forever. In the case of a shock wave, the fact that the characteristics converge into the shock counteracts the smearing, and a steady progressing profile is obtained.

The above observation is the basis for the artificial compression concept [3]. In order to prevent the excessive smearing of a linear discontinuity one can artificially induce convergence of the numerical characteristic field at each monotone strip of the solution. This can be accomplished by modifying the expression of the slopes S^n_j or by adding a corrective term to the numerical flux (1.11) (see [4]). The main advantage of artificial compression is that it is easy to use. The primary disadvantage is that one has to be extra careful (which also means to do a lot of checking...) not to generate unphysical discontinuities by applying it too strongly, where it need not be applied at all.

The piecewise-parabolic method (PPM) of Colella and Woodward [1] includes a mechanism to detect contact discontinuities and to correct the scheme by using a "steeper" reconstruction. The PPM proved itself to be a robust high resolution scheme in a large number of numerical tests [11]. In this paper we present a technique, which we call "subcell resolution," that is close in spirit to the PPM but is somewhat different in its methodology.

The present scheme is a "souped up" version of (1.11) in which the linear advection part is boosted to third-order accuracy (in L_1-sense) and is capable of propagating *linear* discontinuities perfectly (within third-order accuracy). The main ingredient in the new method is the observation that the information in

cell-averages of a discontinuous function, unlike that of point values, contains the location of the discontinuity within the cell, e.g., the cell-averages $\bar{w}_j$,

$$\bar{w}_j = \begin{cases} u_L, & j \leqslant -1 \\ u_M, & j = 0 \\ u_R, & j \geqslant 1, \end{cases} \tag{1.12a}$$

with u_M between u_L and u_R, are identical to those of the step-function

$$w(x) = \begin{cases} u_L & x < (\theta - \frac{1}{2})h \\ u_R & x > (\theta - \frac{1}{2})h, \quad \theta = (u_R - u_M)/(u_R - u_L). \end{cases} \tag{1.12b}$$

Using this observation we can modify the ENO reconstruction of [7] to recover exactly any discontinuous quadratic function from its cell-averages.

In order to retain the relative simplicity of the numerical scheme (1.11) we use the new reconstruction to correct only the linear advection part. The new numerical flux is

$$\hat{f}_{j+1/2} = \hat{f}^{\mathrm{ENO}}_{j+1/2} + \hat{g}_{j+1/2}; \tag{1.13}$$

here $\hat{g}_{j+1/2}$ is the flux through $x_{j+1/2}$ due to the linear advection of the *difference* between the modified reconstruction and the piecewise-linear one (1.9). In the constant coefficient case the scheme (1.13) is exact for discontinuous quadratic initial data.

Later on in this paper we present the extension of the "subcell resolution" concept to any finite order of accuracy and also extend the scheme to the Euler equations of gas dynamics.

2. ENO Reconstruction

In this section, we describe one of the techniques to obtain an ENO reconstruction. Given cell-averages $\{\bar{w}_j\}$ of a piecewise smooth function $w(x)$, we observe that

$$h\bar{w}_j = \int_{x_{j-1/2}}^{x_{j+1/2}} w(y)\,dy = W(x_{j+1/2}) - W(x_{j-1/2}), \tag{2.1a}$$

where

$$W(x) = \int_{x_0}^{x} w(y)\,dy \tag{2.1b}$$

is the primitive function of $w(x)$. Hence we can easily compute the *point values* $\{W(x_{i+1/2})\}$ by summation

$$W(x_{i+1/2}) = h \sum_{j=i_0}^{i} \bar{w}_j. \tag{2.2}$$

Let $H_m(x; u)$ be an interpolation of u at the points $\{y_j\}$, which is accurate to order m, i.e.,

$$H_m(y_j; u) = u(y_j), \tag{2.3a}$$

$$\frac{d^l}{dx^l} H_m(x; u) = \frac{d^l}{dx^l} u(x) + O(h^{m+1-l}), \qquad 0 \leqslant l \leqslant m. \tag{2.3b}$$

We obtain our "reconstruction via primitive function" technique by defining

$$R(x; \bar{w}) = \frac{d}{dx} H_r(x; W). \tag{2.4}$$

Relation (1.6a) follows immediately from (2.3b) with $l = 1$ and the definition (2.1); i.e.,

$$\begin{aligned} R(x; \bar{w}) &= \frac{d}{dx} H_r(x; W) = \frac{d}{dx} W(x) + O(h^r) \\ &= w(x) + O(h^r). \end{aligned}$$

Relation (1.6b) is a direct consequence of (2.3a) and (2.2); i.e.,

$$\begin{aligned} A(I_j) R(\cdot; \bar{w}) &= \frac{1}{h} \int_{x_{j-1/2}}^{x_{j+1/2}} \frac{d}{dx} H_r(x, W)\, dx \\ &= \frac{1}{h} [H_r(x_{j+1/2}; W) - H_r(x_{j-1/2}; W] \\ &= \frac{1}{h} [W(x_{j+1/2}) - W(x_{j-1/2})] = \bar{w}_j. \end{aligned}$$

To obtain an ENO reconstruction, we take H_r in (2.4) to be the new ENO interpolation technique of the author [5]. In this case, $H_m(x; u)$ is a piecewise-polynomial function of x of degree m, which is defined (omitting the u dependence) by

$$H_m(x; u) = q_{j+1/2}(x) \qquad \text{for} \quad y_j \leqslant y \leqslant y_{j+1}, \tag{2.5a}$$

where $q_{j+1/2}$ is the unique polynomial of degree m that interpolates u at the $m+1$ points

$$S_m(i) \equiv \{y_{i+1}, \ldots, y_{i+m}\} \tag{2.5b}$$

for a particular choice of $i = i(j)$ (to be described in the following). To satisfy (2.3a), we need

$$q_{j+1/2}(y_j) = u(y_j), \qquad q_{j+1/2}(y_{j+1}) = u(y_{j+1});$$

therefore, we limit our choice of $i(j)$ to

$$j-m+1 \leqslant i(j) \leqslant j. \tag{2.5c}$$

The ENO interpolation technique is nonlinear: At each interval $[y_j, y_{j+1}]$, we consider the m possible choices of stencils (2.5b) subject to the restriction (2.5c) and assign to this interval the stencil in which u is "smoothest" in some sense; this is done by specifying $i(j)$ in (2.5b).

The information about the smoothness of u can be extracted from a table of divided differences. The kth divided difference of u,

$$u[y_i, y_{i+1}, \ldots, y_{i+k}] \equiv u[S_k(i)], \tag{2.6a}$$

is defined inductively by

$$u[S_0(i)] = u(y_i) \tag{2.6b}$$

and

$$u[S_k(i)] = (u[S_{k-1}(i+1)] - u[S_{k-1}(i)])/(y_{i+k} - y_i). \tag{2.6c}$$

If $u(x)$ is m times differentiable in $[y_i, y_{i+m}]$ then

$$u[S_m(i)] = \frac{1}{m!} u^{(m)}(\xi), \qquad \text{for some} \quad y_i \leqslant \xi \leqslant y_{i+m}. \tag{2.7a}$$

If $u^{(p)}(x)$ has a jump discontinuity in $[y_i, y_{i+m}]$ then

$$u[S_m(i)] = O(h^{-m+p}[u^{(p)}]), \qquad 0 \leqslant p \leqslant m-1 \tag{2.7b}$$

($[u^{(p)}]$ in the RHS of (2.7b) denotes the jump in the pth derivative).

Relations (2.7) show that $|u[S_m(i)]|$ is a measure of the smoothness of u in $S_m(i)$ and therefore can serve as a tool to compare the relative smoothness of u in various stencils. The simplest algorithm to assign $S_m(i(j))$ to the interval $[y_j, y_{j+1}]$ is the following:

ALGORITHM I. Choose $i(j)$ so that

$$|u[S_m(i(j))]| = \min_{j-m+1 \leqslant i \leqslant j} \{|u[S_m(i)]|\}. \tag{2.8}$$

Clearly (2.8) selects the "smoothest" stencil, provided that h is sufficiently small.

In order to make a sensible selection of stencil also when h is not sufficiently small, i.e., in the "pre-asymptotic" case, we prefer to use the following hierarchial algorithm:

ALGORITHM II. Let $i_k(j)$ be such that $S_k(i_k(j))$ is our choice of a $(k+1)$-point stencil for $[y_j, y_{j+1}]$. Obviously, we have to set

$$i_1(j) = j \tag{2.9a}$$

To choose $i_{k+1}(j)$, we consider as candidates the two stencils

$$S^L_{k+1} = S_{k+1}(i_k(j) - 1), \tag{2.9b}$$

$$S^R_{k+1} = S_{k+1}(i_k(j)), \tag{2.9c}$$

which are obtained by adding a point to the left of (or to the right of) $S_k(i_k(j))$, respectively. We select the one in which u is relatively smoother, i.e.,

$$i_{k+1}(j) = \begin{cases} i_k(j) - 1 & \text{if } |u[S^L_{k+1}]| < |u[S^R_{k+1}]| \\ i_k(j) & \text{otherwise.} \end{cases} \tag{2.9d}$$

Finaly, we set $i(j) = i_m(j)$.

Using Newton's form of interpolation, we see that the polynomials $\{q_k(x)\}$, $1 \leqslant k \leqslant m$, corresponding to the stencils $S^k = S_k(i_k(j))$ selected by Algorithm II, satisfy the relation

$$q_{k+1}(x) = q_k(x) + u[S^{k+1}] \prod_{y \in S^k} (x - y). \tag{2.9e}$$

This shows that the choice made in (2.9d) selects q_{k+1} to be the one that deviates the least from q_k. It is this property that makes Algorithm II meaningful also for h in the pre-asymptotic range.

3. ENO RECONSTRUCTION WITH SUBCELL RESOLUTION

In this section, we show how to modify the ENO reconstruction of the previous section so as to allow for the recovery of discontinuities in the interior of the cells. To illustrate the procedure, we first consider a discontinuous piecewise polynomial function $w(x)$ of the form

$$w(x) = \begin{cases} P_L(x), & x < x_d \\ P_R(x), & x > x_d, \end{cases} \tag{3.1a}$$

where $P_L(x)$ and $P_R(x)$ are polynomials of degree less than or equal to s,

$$\deg(P_L) \leqslant s, \qquad \deg(P_R) \leqslant s. \tag{3.1b}$$

We assume that $w(x)$ is actually discontinuous at x_d, i.e.,

$$P_L(x_d) \neq P_R(x_d) \tag{3.1c}$$

and that the discontinuity is located in the interior of the interval I_0

$$x_{-1/2} < x_d < x_{1/2}. \tag{3.1d}$$

(See Fig. 1a.)

Next we denote the cell-averages of $w(x)$ in (3.1) by $\{\bar{w}_j\}$ and consider the ENO reconstruction $R(x; \bar{w})$ applied to these data. To simplify our presentation let us denote the polynomial defining $R(x; \bar{w})$ in the cell I_j by $R_j(x; \bar{w})$. Clearly, provided h is sufficiently small, the stencils assigned to cells $\{I_k\}$, $j \neq 0$, are selected from the smooth part of the function. Therefore it follows from (2.3)–(2.5) that

$$\begin{aligned} R_j(x; \bar{w}) &= P_L(x) + O(h^r) \qquad \text{for} \quad j \leqslant -1 \\ R_j(x; \bar{w}) &= P_R(x) + O(h^r) \qquad \text{for} \quad j \geqslant 1. \end{aligned} \tag{3.2}$$

$R(x; \bar{w})$ in I_0 does not introduce spurious oscillations; however, it does not provide an accurte approximation to the discontinuous function $w(x)$ either (see Fig. 1b). Using (3.2) and the information contained in the cell-average $\bar{w}_0$, we can easily rectify this situation as follows: We extend $R_{-1}(x; \bar{w})$ to a point z in I_0 from the left, and extend $R_1(x; \bar{w})$ to z from the right and then approximate the location of the discontinuity in the cell I_0 by finding a value of z that will fit the cell average $\bar{w}_0$ (see Fig. 1c). This is done by finding a root of the algebraic equation $F_0(z) = 0$, where

$$F_0(z) = \frac{1}{h}\left\{\int_{x_{-1/2}}^{z} R_{-1}(x; \bar{w})\, dx + \int_{z}^{x_{1/2}} R_1(x; \bar{w})\, dx\right\} - \bar{w}_0. \tag{3.3a}$$

When h is sufficiently small, the data near the cell I_0 approach those of a step-function. Therefore, as in (1.12) we expect to have

$$F_0(x_{-1/2}) \cdot F_0(x_{1/2}) \leqslant 0 \tag{3.3b}$$

and a single root of $F_0(z) = 0$ in I_0; we denote this root by θ_0,

$$F_0(\theta_0) = 0. \tag{3.3c}$$

It follows from (3.2) that

$$|\theta_0 - x_d| = O(h^r). \tag{3.3d}$$

What we mean by "ENO reconstruction with subcell resolution" is the modified ENO reconstruction $\hat{R}(x; \bar{w})$ which is defined in this case by

$$\hat{R}_j(x; \bar{w}) = R_j(x; \bar{w}) \qquad \text{for} \quad j \neq 0 \tag{3.4a}$$

$$\hat{R}(x; \bar{w}) = \begin{cases} R_{-1}(x; \bar{w} & \text{for} \quad x_{-1/2} < x < \theta_0 \\ R_1(x; \bar{w}) & \text{for} \quad \theta_0 < x < x_{1/2}. \end{cases} \tag{3.4b}$$

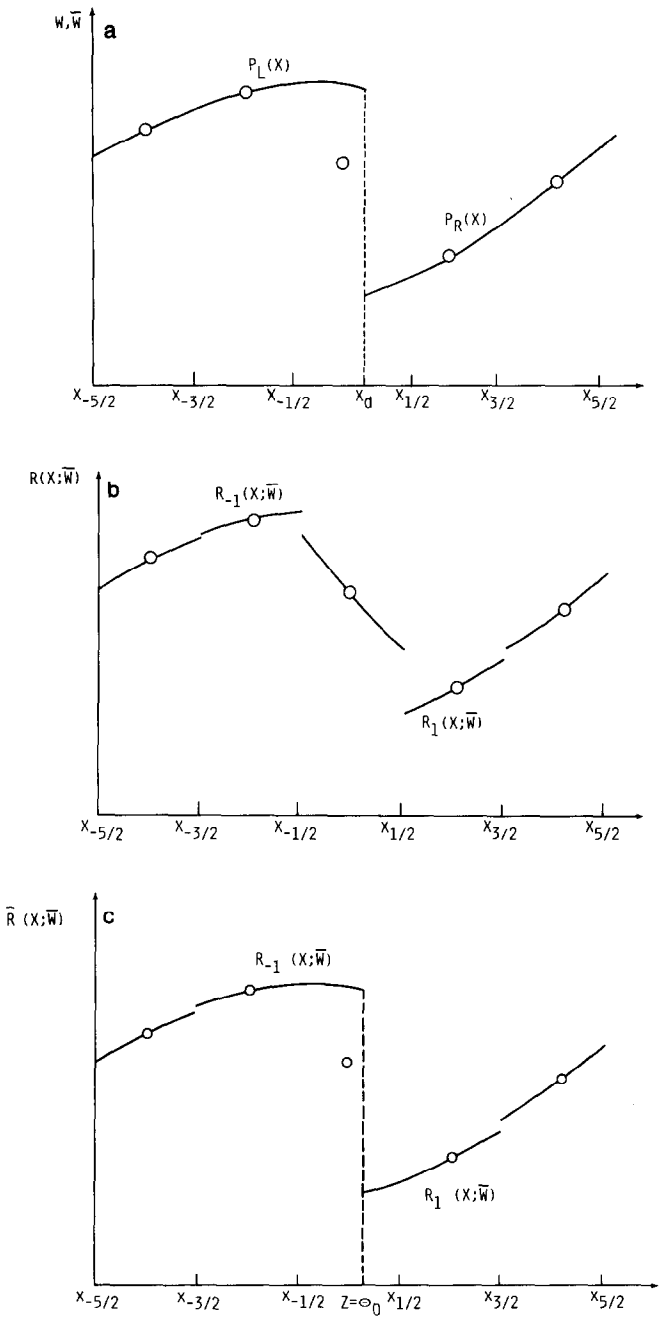

FIG. 1. (a) $w(x)$ in (3.1); circles denote cell-averages $\{\bar{w}_j\}$. (b) The ENO reconstruction $R(x; \bar{w})$. The circles denote the given values of the cell-averages $\{\bar{w}_j\}$. (c) The modified ENO reconstruction with subcelle resolution $\hat{R}(x; \bar{w})$ (3.4). The circles denote the given values of the cell-averages $\{\bar{w}_j\}$.

Clearly it follows from (3.2) and (3.3d) that $\hat{R}(x;\bar{w})$ is an $O(h^r)$ approximation to $w(x)$ in the L_1 sense, i.e., for any a and b,

$$\int_a^b |\hat{R}(x;\bar{w}) - w(x)|\,dx = O(h^r). \tag{3.5}$$

We observe that if the polynomial degree s in (3.1b) is less or equal $(r-1)$ then the primitive functions of P_L and P_R are polynomials of degree les or equal r, and therefore $H_r(x;w)$ in (2.5) is exact except at I_0. Hence,

$$R_j(x;\bar{w}) = P_L(x) \qquad \text{for} \quad j \leqslant -1 \tag{3.6a}$$

$$R_j(x;\bar{w}) = P_R(x) \qquad \text{for} \quad j \geqslant 1, \tag{3.6b}$$

and consequently $\theta_0 = x_d$ in (3.3). Thus we have shown

$$s \leqslant r-1 \Rightarrow \hat{R}(x;\bar{w}) \equiv \bar{w}(x). \tag{3.6c}$$

We turn now to describe the algorithm defining $\hat{R}(x;\bar{w})$ for a general piecewise-smooth function $w(x)$. As in the previous example we take $\hat{R}(x;\bar{w})$ in I_j to be $R_j(x;\bar{w})$, unless I_j is suspected of having a discontinuity of $w(x)$ in its interior. In the latter case we check whether

$$F_j(x_{j-1/2}) \cdot F_j(x_{j+1/2}) \leqslant 0, \tag{3.7a}$$

where

$$F_j(z) = \frac{1}{h}\left\{\int_{x_{j-1/2}}^{z} R_{j-1}(x;\bar{w})\,dx + \int_{z}^{x_{j+1/2}} R_{j+1}(x;\bar{w})\,dx\right\} - \bar{w}_j. \tag{3.7b}$$

If (3.7a) holds, then there is a root $z = \theta_j$,

$$F_j(\theta_j) = 0, \qquad x_{j-1/2} \leqslant \theta_j \leqslant x_{j+1/2} \tag{3.7c}$$

in the cell I_j, and we define $\hat{R}(x;\bar{w})$ in this cell to be

$$\hat{R}_j(x;\bar{w}) = \begin{cases} R_{j-1}(x;\bar{w}) & \text{for} \quad x_{j-1/2} < x < \theta_j \\ R_{j+1}(x;\bar{w}) & \text{for} \quad \theta_j < x < x_{j+1/2}. \end{cases} \tag{3.7d}$$

If (3.7a) does not hold (which means that either there is no root in I_j or that there is an even number of roots in I_j), we take $\hat{R}_j(x;\bar{w})$ to be $R_j(x;\bar{w})$.

Let σ_j be some measure of the non-smoothness of the reconstruction $R(x;\bar{w})$ in I_j, e.g.,

$$\sigma_j = \left|\frac{d^k}{dx^k} R(x_j;\bar{w})\right|, \qquad 1 \leqslant k \leqslant r-1, \tag{3.8a}$$

or a combination of such derivatives. Our algorithm identifies cells which are

suspect of harboring a discontinuity of $w(x)$, as those which attain a local maximum of "non-smoothness" of the reconstruction, i.e.,

$$\sigma_j > \sigma_{j-1} \quad \text{and} \quad \sigma_j \geqslant \sigma_{j+1}. \tag{3.8b}$$

We summarize the algorithm defining $\hat{R}(x; \bar{w})$ by: If

$$\sigma_j > \sigma_{j-1}, \quad \sigma_j \geqslant \sigma_{j+1} \quad \text{and} \quad F_j(x_{j-1/2}) \cdot F_j(x_{j+1/2}) \leqslant 0 \tag{3.9a}$$

then

$$\hat{R}_j(x; \bar{w}) = \begin{cases} R_{j-1}(x; \bar{w}) & \text{for} \quad x_{j-1/2} < x < \theta_j \\ R_{j+1}(x; \bar{w}) & \text{for} \quad \theta_j < x < x_{j+1/2}; \end{cases} \tag{3.9b}$$

otherwise,

$$\hat{R}_j(x; \bar{w}) = R_j(x; \bar{w}). \tag{3.9c}$$

In an Appendix, we present analysis which motivates the choice of condition (3.8b). In the following we make several remarks and observations about $\hat{R}(x; w)$, the "ENO reconstruction with subcell resolution."

(1) $\hat{R}(x; \bar{w})$ is indeed essentially non-oscillatory (ENO). This follows from the fact that local maxima are isolated; i.e., if (3.8b) holds for I_j, it cannot hold either for I_{j-1} or for I_{j+1}. Consequently, if $\hat{R}(x; \bar{w})$ is defined in I_j by the discontinuous (3.9b), then in I_{j-1} and I_{j+1} it is defined by (3.9c); i.e.,

$$\hat{R}_{j-1}(x; \bar{w}) = R_{j-1}(x; \bar{w}), \qquad \hat{R}_{j+1}(x; \bar{w}) = R_{j+1}(x; \bar{w}). \tag{3.10}$$

(2) If, as in the example (3.1), there is a discontinuity of $w(x)$ in the interior of I_0, then

$$\sigma_0 = O(h^{-k}), \qquad \sigma_{-1} = O(1), \qquad \sigma_1 = O(1), \tag{3.11a}$$

where k is the order of the derivative used in (3.8a).

Therefore, provided h is sufficiently small, we get that

$$\sigma_0 > \sigma_{-1}, \qquad \sigma_0 > \sigma_1, \tag{3.11b}$$

and also as in (3.3b),

$$F_0(x_{-1/2}) \cdot F_0(x_{1/2}) < 0. \tag{3.11c}$$

This shows that $\hat{R}(x; \bar{w})$, as defined by the general algorithm (3.9), will recover any real discontinuity of $w(x)$.

(3) We observe that condition (3.9a) may hold also in the smooth part of $w(x)$ near a local maximum of $|d^k w/dx^k|$. In this case the algorithm places a discon-

tinuity at θ_j in the interior of I_j. However, because of the smoothness of $w(x)$ there and (1.6a), we have

$$R_{j\pm 1}(\theta_j; \bar{w}) = w(\theta_j) + O(h^r). \tag{3.12}$$

Consequently the jump is of the size of the reconstruction error $O(h^r)$. We recall that the original ENO reconstruction is discontinuous at $\{x_{j+1/2}\}$. Therefore, the effect of the algorithm (3.9) is to replace the two discontinuities at $x_{j-1/2}$ and $x_{j+1/2}$ by a single one at θ_j.

(4) We observe that in order to evaluate $\hat{R}_j(x; \bar{w})$ in a cell I_j which contains a discontinuity at θ_j, we have to find out whether $x > \theta_j$ or $x < \theta_j$. Assuming θ_j to be the only root of $F_j(\theta_j) = 0$ in I_j, as is the case for a real discontinuity, we can use the logic of the interval-halving technique to evaluate $\hat{R}_j(x; \bar{w})$ without actually computing θ_j. To do so we calculate $F_j(x)$ and compare its sign with that of $F_j(x_{j-1/2})$ or $F_j(x_{j+1/2})$:

$$\hat{R}_j(x; \bar{w}) = \begin{cases} R_{j-1}(x; \bar{w}) & \text{if } F_j(x) \cdot F_j(x_{j-1/2}) > 0 \\ R_{j+1}(x; \bar{w}) & \text{otherwise.} \end{cases} \tag{3.13}$$

4. A Second-Order Accurate ENO Scheme with Subcell Resolution

In the following we describe how to incorporate the reconstruction with subcell resolution into the ENO schemes, so as to improve their resolution of linear discontinuities. In this section, we present the derivation of (1.13), which is an improved version of the second-order accurate MUSCL-type scheme (1.11). In the next section, we shall generalize these ideas to any order of accuracy.

We start with the piecewise-parabolic reconstruction $R(x; \bar{w})$ which is defined by (2.4) with $r = 3$, i.e.,

$$R(x; \bar{w}) = \frac{d}{dx} H_3(x; W), \tag{4.1a}$$

where W is the primitive function (2.1b) of $w(x)$, and $H_3(x; W)$ is a piecewise-cubic ENO interpolation. Let $i = i(j)$ be the left endpoint of the stencil $(x_{i-1/2}, x_{i+1/2}, x_{i+3/2}, x_{i+5/2})$ assigned to the interval $(x_{j-1/2}, x_{j+1/2})$ by (2.8) or (2.9) or some other ENO technique; $j-2 \leqslant i \leqslant j$. The parabola describing $R(x; \bar{w})$ in $(x_{j-1/2}, x_{j+1/2})$ is given by

$$C_j = \frac{d^3 H_3(x; W)}{dx^3} = (\bar{w}_{i+2} - 2\bar{w}_{i+1} + \bar{w}_i)/h^2 \tag{4.1b}$$

$$S_j = \left.\frac{d^2 H_3(x; w)}{dx^2}\right|_{x = x_j} = (\bar{w}_{i+1} - \bar{w}_i)/h + \left(j - i - \frac{1}{2}\right) hC_j \tag{4.1c}$$

$$R(x; \bar{w}) = \left(\bar{w}_j - \frac{h^2}{24} C_j\right) + S_j(x - x_j) + \frac{1}{2} C_j (x - x_j)^2. \tag{4.1d}$$

Our basic scheme remains

$$v_j^{n+1} = A(I_j)E(\tau)L(\cdot; v^n) \tag{4.2a}$$

with the piecewise linear reconstruction

$$L(x; \bar{w}) = \bar{w}_j + S_j(x - x_j), \qquad x \in I_j, \tag{4.2b}$$

but we use the parabolic reconstruction in order to define the slope S_j by (4.1c); as in (1.11) we approximate its numerical flux by

$$\hat{f}_{j+1/2} = \hat{f}^{\mathrm{ENO}}_{j+1/2} = f^R(v^L_{j+1/2}, v^R_{j+1/2}), \tag{4.3a}$$

where

$$v^L_{j+1/2} = v_j^n + h(1 - \lambda a_j^n)S_j^n/2, \qquad v^R_{j+1/2} = v^n_{j+1} - h(1 + \lambda a^n_{j+1})S_{j+1}/2. \tag{4.3b}$$

We observe that by (2.3b) choosing S_j(in (4.4b) to be (4.1c) results in

$$S_j = w_x(x_j) + O(h^2), \tag{4.3c}$$

which is one order higher than (1.9b). Consequently, as the UNO scheme of Harten and Osher [6], this scheme is truly second order in all L_p norms (unlike TVD schemes which are first order in L_∞ and second order only in L_1).

Using the algorithm described in (3.9) we now define $\hat{R}(x; \bar{w})$, which modifies $R(x; \bar{w})$ in (4.1) so that it includes a discontinuity in the interior of each cell I_j which meets condition (3.9a). Ideally, we would like to use the scheme

$$v_j^{n+1} = A(I_j)E(\tau)\hat{R}(\cdot; v^n), \tag{4.4}$$

which is third-order accurate in L_1-sense (but only second-order accurate in the maximum norm). However, the proper approximation of the numerial flux of (4.2) is more complicated than (1.11), since it is one order more accurate in time. Bearing in mind that the main fault in the MUSCL-type scheme (1.11) that we want to correct is the smearing of linear discontinuities, we introduce subcell resolution into the scheme by correcting its numerical flux to account for the difference between using $\hat{R}$ and L in the constant coefficient case. Thus we use the scheme

$$v_j^{n+1} = v_j^n - \lambda(\hat{f}_{j+1/2} - \hat{f}_{j-1/2}) \tag{4.5a}$$

$$\hat{f}_{j+1/2} = \hat{f}^{\mathrm{ENO}}_{j+1/2} + \hat{g}_{j+1/2}, \tag{4.5b}$$

and define $\hat{g}_{j+1/2}$ by the requirement that the scheme (4.5) becomes identical to (4.4) in the constant coefficient case

$$u_t + au_x = 0, \qquad a = \text{const.} \tag{4.6}$$

This determines $\hat{g}_{j+1/2}$ to be

$$\hat{g}_{j+1/2}=\frac{a}{\tau}\int_0^\tau [\hat{R}(x_{j+1/2}-at;v^n)-L(x_{j+1/2}-at;v^n)]\,dt. \tag{4.7a}$$

Since in the constant coefficient case

$$f^{\mathrm{ENO}}_{j+1/2}=\frac{a}{\tau}\int_0^\tau L(x_{j+1/2}-at;v^n)\,dt, \tag{4.7b}$$

we get that

$$f_{j+1/2}=\frac{a}{\tau}\int_0^\tau \hat{R}(x_{j+1/2}-at;v^n)\,dt. \tag{4.7c}$$

which shows that the scheme (4.5) is indeed identical to (4.4) in the constant coefficient case (4.6). Consequently, it is exact for discontinuous parabolic data of the form (3.1).

Next we derive an expression for $\hat{g}_{j+1/2}$ in the constant coefficient case (4.7a); this will later be generalized to the nonlinear case by "freezing" the characteristic speed within the cell.

In the constant coefficient case, (4.7a) can be rewritten as

$$\hat{g}_{j+1/2}=\frac{1}{\tau}\int_{x_{j+1/2}-a\tau}^{x_{j+1/2}} [\hat{R}(y;v^n)-L(y;v^n)]\,dy. \tag{4.8}$$

First let us assume $a>0$. When

$$\hat{R}(x;v^n)=R_j(x;v^n) \qquad \text{in } I_j, \tag{4.9a}$$

then

$$\hat{g}_{j+1/2}=\frac{1}{\tau}\int_{x_{j+1/2}-a\tau}^{x_{j+1/2}} [R_j(y;v^n)-L(y;v^n)]\,dy=\frac{a}{12}(\nu-1)(2\nu-1)h^2C_j; \tag{4.9b}$$

here $\nu=\lambda a$.

When there is a discontinuity in the interior of I_j, $\hat{R}_j(x;v^n)$ is given by (3.9b); i.e.,

$$\hat{R}(x;v^n)=\begin{cases}R_{j-1}(x;v^n), & x_{j-1/2}\leqslant x<\theta_j\\ R_{j+1}(x;v^n), & \theta_j\leqslant x\leqslant x_{j+1/2},\end{cases} \tag{4.10a}$$

and we have to find out whether $(x_{j+1/2}-a\tau)$ is larger or smaller than θ_j. We recall that for (4.10a) to hold the relations

$$F_j(\theta_j)=0, \qquad F_j(x_{j-1/2})\cdot F_j(x_{j+1/2})\leqslant 0 \tag{4.10b}$$

have to be satisfied, where $F_j(z)$ is defined by (3.7b). Using the basic idea of the interval-halving method for calculating a root of algebraic equations, we can find out in which of the two cases we are without actually calculating θ_j (see Remark (4)

at the end of the previous section). All we have to do is to compute $F_j(x_{j+1/2}-a\tau)$ and compare its sign to that of $F_j(x_{j-1/2})$, i.e.,

$$F_j(x_{j+1/2}-a\tau)\cdot F_j(x_{j-1/2})>0 \Rightarrow x_{j+1/2}-a\tau<\theta_j \tag{4.10c}$$

$$F_j(x_{j+1/2}-a\tau)\cdot F_j(x_{j-1/2})\leqslant 0 \Rightarrow x_{j+1/2}-a\tau\geqslant\theta_j. \tag{4.10d}$$

To express the integral in (4.8) let us introduce the notation

$$b_m(y_1, y_2)=\int_{y_1}^{y_2} R_m(x; v^n)\,dx=\left[\left(v_m^n-\frac{h^2}{24}C_m\right)y+\frac{1}{2}S_m y^2+\frac{1}{6}C_m y^3\right]_{y_1-x_m}^{y_2-x_m}. \tag{4.11}$$

In case $x_{j+1/2}-a\tau\geqslant\theta_j$, we get from (4.8) and (4.10a) that

$$\hat{g}_{j+1/2}=\frac{1}{\tau}\left\{b_{j+1}(x_{j+1/2}-a\tau, x_{j+1/2})-a\tau\left[v_j^n+\frac{1}{2}(h-a\tau)S_j^n\right]\right\}. \tag{4.12a}$$

When $x_{j+1/2}-a\tau<\theta_j$, we use the fact that

$$\frac{1}{h}\int_{x_{j-1/2}}^{x_{j+1/2}}\hat{R}(x; v^n)\,dx=v_j^n$$

to express the integral in (4.8) by

$$\int_{x_{j+1/2}-a\tau}^{x_{j+1/2}}\hat{R}(x; v^n)\,dx=hv_j^n-\int_{x_{j-1/2}}^{x_{j+1/2}-a\tau}\hat{R}(x; v^n)\,dx$$

$$=hv_j^n-\int_{x_{j-1/2}}^{x_{j+1/2}-a\tau}R_{j-1}(x; v^n)\,dx.$$

Rearranging terms we get in this case

$$\hat{g}_{j+1/2}=\frac{1}{\tau}\left\{(h-a\tau)\left(v_j^n-\frac{a\tau}{2}S_j^n\right)-b_{j-1}(x_{j-1/2}, x_{j+1/2}-a\tau)\right\}. \tag{4.12b}$$

To summarize, the definition of $\hat{g}_{j+1/2}$ in the case $a>0$ is

$$\tau\hat{g}_{j+1/2}=\frac{a\tau}{12}(\nu-1)(2\nu-1)h^2C_j, \tag{4.13a}^+$$

unless the discontinuity condition (3.9a) holds for I_j; in the latter case we define

$$\tau\hat{g}_{j+1/2}=\begin{cases}(h-a\tau)\left(v_j^n-\dfrac{a\tau}{2}S_j\right)-b_j(x_{j-1/2}, x_{j+1/2}-a\tau)\\ \qquad\qquad\text{if}\quad F_j(x_{j+1/2}-a\tau)\cdot F_j(x_{j-1/2})>0\\ b_{j+1}(x_{j+1/2}-a\tau, x_{j+1/2})-a\tau[v_j^n+\frac{1}{2}(h-a\tau)S_j]\\ \qquad\qquad\text{otherwise.}\end{cases} \tag{4.13b}^+$$

Similarly for $a<0$ we get

$$\tau\hat{g}_{j-1/2}=\frac{a\tau}{12}(\nu+1)(2\nu+1)h^2C_j, \tag{4.13a}^-$$

unless the discontinuity condition (3.9a) holds for I_j; in the latter case we define

$$\tau\hat{g}_{j-1/2}=\begin{cases} -b_{j-1}(x_{j-1/2},\, x_{j-1/2}-a\tau)-a\tau[v_j^n-\frac{1}{2}(h+a\tau)]S_j \\ \qquad\qquad \text{if} \quad F_j(x_{j-1/2})\cdot F_j(x_{j-1/2}-a\tau)>0 \\ b_{j+1}(x_{j-1/2}-a\tau,\, x_{j+1/2})-(h+a\tau)\left(v_j^n-\dfrac{a\tau}{2}S_j\right) \\ \qquad\qquad \text{otherwise.} \end{cases} \tag{4.13b}^-$$

Note that the expressions (4.13) are formulated as the contribution of the cell I_j to the numerical flux $\hat{g}$. Thus, if $a>0$, the contribution of from the I_j cell goes to $\hat{g}_{j+1/2}$, while if $a<0$ this contribution goes to $\hat{g}_{j-1/2}$.

In Section 6, we extend the subcell resolution ideas to the Euler equations of gas dynamics. Since shocks are highly resolved by the original ENO scheme, we apply subcell resolution only to the linearly degenerate characteristic field in order to improve the resolution of contact discontinuities. In this case the characteristic speed, which is the velocity of the flow, is not a constant but a function of the solution itself. Nevertheless, we use the same expressions as in (4.13), except that a in I_j is replaced by a_j, and $\nu=\lambda a_j$. We compute the corrective flux $\hat{g}$ in the following way: First we preset $\hat{g}=0$, and then we sweep over the mesh and collect contributions to $\hat{g}$ from each cell: If $a_j>0$ we add the RHS of $(4.13)^+$ to $\hat{g}_{j+1/2}$; if $a_j<0$ we add the RHS of $(4.13)^-$ to $\hat{g}_{j-1/2}$. Note that if $a_{j+1}<0$ and $a_j>0$, then $\hat{g}_{j+1/2}$ gets contributions from both I_j and I_{j+1}.

5. Extension to High Order of Accuracy

In this section, we describe the extension of the ENO scheme with subcell resolution to arbitrarily high order of accuracy. As in the second-order case (4.5), we introduce subcell resolution to the high order accurate ENO schemes via a corrective flux $\hat{g}_{j+1/2}$; i.e., we consider the modified scheme

$$v_j^{n+1}=v_j^n-\lambda(\tilde{f}_{j+1/2}-\tilde{f}_{j-1/2}) \tag{5.1a}$$

$$\tilde{f}_{j+1/2}=f_{j+1/2}^{\mathrm{ENO}}+\hat{g}_{j+1/2}. \tag{5.1b}$$

First, we describe briefly the derivation of $f_{j+1/2}^{\mathrm{ENO}}$. We refer the reader to [7] for more details. Let $L(x;\bar{w})$ be an rth order accurate reconstruction of $w(x)$, such that

$$\frac{1}{h}\int_{I_j}L(x;\bar{w})\,dx=\bar{w}_j. \tag{5.2a}$$

As before we denote the $(r-1)$th degree polynomial describing $L(x; \bar{w})$ in I_j by $L_j(x; \bar{w})$, and express it in the following Taylor expansion

$$L_j(x; \bar{w}) = \sum_{k=0}^{r-1} \frac{\tilde{D}_k}{k!} (x - x_j)^k, \qquad \tilde{D}_k = \frac{d^k}{dx^k} L(x_j; \bar{w}). \tag{5.2b}$$

Let $u_j(x, t)$ be the solution to the initial value problem

$$u_t + f(u)_x = 0, \qquad u(x, 0) = L_j(x; \bar{w}). \tag{5.3a}$$

Since the initial data in (5.3a) are analytic, we know from the Cauchy–Kowalewski theorem that $u_j(x, t)$ exists uniquely and it is analytic for some time $0 \leqslant t \leqslant t_c$. Therefore, its Taylor expansion around $x = x_j$ and $t = 0$

$$u_j(x, t) = \sum_{k=0}^{\infty} \frac{1}{k!} \sum_{m=0}^{k} \binom{k}{m} \tilde{D}_{m,k-m} t^m (x - x_j)^{k-m}, \tag{5.3b}$$

$$\tilde{D}_{m,k-m} = \frac{\partial^k}{\partial t^m \partial x^{k-m}} u_j(x_j, 0), \tag{5.3c}$$

is valid for $0 \leqslant t \leqslant t_c$ and x sufficiently close to x_j. Using (5.3) we define $v_j(x, t)$ to be the truncated Taylor expansion

$$v_j(x, t) = \sum_{k=0}^{r-1} \frac{1}{k!} \sum_{m=0}^{k} \binom{k}{m} \tilde{D}_{m,k-m} t^m (x - x_j)^{k-m}, \tag{5.4a}$$

$$|v_j(x, t) - u_j(x, t)| = O(h^r). \tag{5.4b}$$

The coefficients $\tilde{D}_{m,k-m}$ in (5.4a) can be computed directly from the known coefficients $\{\tilde{D}_k\}$ in (5.2b) (note that $\tilde{D}_{0,k} = \tilde{D}_k$) by successive differentiation of the partial differential equation and substitution—see [7] for details.

Finally, using an appropriate numerical quadrature to approximate the integral in (1.5a), we define $f^{\text{ENO}}_{j+1/2}$ to be

$$f^{\text{ENO}}_{j+1/2} = \sum_{k=1}^{K} \beta_k f^R(v_j(x_{j+1/2}, \gamma_k \tau), v_{j+1}(x_{j+1/2}, \gamma_k \tau)). \tag{5.5}$$

Here β_k and γ_k are the coefficients of the numerical quadrature. In the second-order case we use the midpoint rule: $K = 1$, $\beta_k = 1$, $\gamma_k = \frac{1}{2}$. In the third- and fourth-order case we use the Gaussian quadrature: $K = 2$, $\beta_1 = \beta_2 = \frac{1}{2}$, $\gamma_1 = \frac{1}{2}(1 - 1/\sqrt{3})$, $\gamma_2 = \frac{1}{2}(1 + 1/\sqrt{3})$. Note that the second-order accurate scheme (1.11) is identical to (5.5) with $r = 2$.

Next we describe the derivation of the corrective flux $\hat{g}_{j+1/2}$ in (5.1b). Let $R(x; \bar{w})$ be another reconstruction of $w(x)$ which is at least rth order accurate. Using the

algorithm (3.9) we define $\hat{R}(x; \bar{w})$, its modified version with subcell resolution. As in the second-order case (4.7a) we define $\hat{g}_{j+1/2}$ in the constant coefficient case to be

$$\hat{g}_{j+1/2} = \frac{a}{\tau}\int_0^\tau [\hat{R}(x_{j+1/2} - at; v^n) - L(x_{j+1/2} - at; v^n)]\, dt$$

$$= \frac{1}{\tau}\int_{x_{j+1/2}-a\tau}^{x_{j+1/2}} [\hat{R}(y; v^n) - L(y; v^n)]\, dy. \tag{5.6}$$

We note that relations (4.7b)–(4.7c) hold for any r; therefore, we can state that the scheme (5.1) in the constant coefficient case is identical to (4.4) in general. Consequently, if the reconstruction $R(x; \bar{w})$ is exact for *smooth* polynomial data of degree r, then the ENO scheme with subcell resolution (5.1) is exact for all initial data of *discontinuous* piecewise-polynomial functions of degree less than or equal to r.

Let us denote

$$d_m(y_1, y_2) = \int_{y_1}^{y_2} [R_m(x; v^n) - L_m(x; v^n)]\, dx, \tag{5.7a}$$

$$C_{m+1/2}(y_1, y_2) = \int_{y_1}^{y_2} [R_{m+1}(x; v^n) - R_m(x; v^n)]\, dx. \tag{5.7b}$$

Using these notations we can evaluate $\hat{g}_{j+1/2}$ by the following expressions:

If $a > 0$, then

$$\tau\hat{g}_{j+1/2} = d_j(x_{j+1/2} - a\tau, x_{j+1/2}), \tag{5.8a}^+$$

unless

$$\sigma_j > \sigma_{j-1}, \quad \sigma_j \geqslant \sigma_{j+1}, \qquad F_j(x_{j+1/2}) \cdot F_j(x_{j-1/2}) \leqslant 0, \tag{5.8b}^+$$

in which case

$$\tau\hat{g}_{j+1/2} = \begin{cases} d_j(x_{j+1/2} - a\tau, x_{j+1/2}) + C_{j+1/2}(x_{j+1/2} - a\tau, x_{j+1/2}) \\ \qquad\qquad \text{if} \quad F_j(x_{j+1/2}) \cdot F_j(x_{j+1/2} - a\tau) > 0 \\ d_j(x_{j+1/2} - a\tau, x_{j+1/2}) + C_{j-1/2}(x_{j-1/2}, x_{j+1/2} - a\tau), \\ \qquad\qquad \text{otherwise.} \end{cases} \tag{5.8c}^+$$

If $a < 0$, then

$$\tau\hat{g}_{j-1/2} = -d_j(x_{j-1/2}, x_{j-1/2} - a\tau), \tag{5.8a}^-$$

unless

$$\sigma_j > \sigma_{j-1}, \quad \sigma_j \geqslant \sigma_{j+1}, \qquad F_j(x_{j+1/2}) \cdot F_j(x_{j-1/2}) \leqslant 0, \tag{5.8b}^-$$

in which case

$$\tau\hat{g}_{j-1/2}=\begin{cases}-d_j(x_{j-1/2},\, x_{j-1/2}-a\tau)+C_{j+1/2}(x_{j-1/2}-a\tau,\, x_{j+1/2}),\\ \qquad\qquad \text{if}\quad F_j(x_{j+1/2})\cdot F_j(x_{j-1/2}-a\tau)>0\\ -d_j(x_{j-1/2},\, x_{j-1/2}-a\tau)+C_{j-1/2}(x_{j-1/2},\, x_{j-1/2}-a\tau),\\ \qquad\qquad \text{otherwise.}\end{cases} \tag{5.8c}^{-}$$

We observe tht up to this point we have not specified $L(x;\bar{w})$ and $R(x;\bar{w})$. One possibility is to generalize the set up of the second-order accurate scheme in Section 3 as follows: Let r be the desired order of accuracy of the scheme. We start with a reconstruction via primitive function $R(x;\bar{w})$ which is one order higher, i.e.,

$$R(x;\bar{w})=\frac{d}{dx}H_{r+1}(x;W); \tag{5.9a}$$

here W is the primitive function of w and H_{r+1} is the ENO interpolation of Section 2. As before we denote the polynomial of degree r defining $R(x;\bar{w})$ in $_j$ by $R_j(x;\bar{w})$ and rewrite (5.9a) as a finite Taylor expansion:

$$R_j(x;\bar{w})=\sum_{k=0}^{r}\frac{D_k}{k!}(x-x_j)^k,\qquad D_k=\frac{d^{k+1}}{dx^{k+1}}H_{r+1}(x_j;W). \tag{5.9b}$$

Using (5.9b) we now define $L(x;\bar{w})$ to be

$$L_j(x;\bar{w})=(D_0+\alpha_r h^r D_r)+\sum_{k=0}^{r-1}\frac{D_k}{k!}(x-x_j)^k, \tag{5.10a}$$

where

$$\alpha_k=\begin{cases}0 & \text{for } k \text{ odd}\\ 2^{-k}/(k+1)! & \text{for } k \text{ even.}\end{cases} \tag{5.10b}$$

$L_j(x;\bar{w})$ is a polynomial of degree $(r-1)$ which reconstructs $w(x)$ in I_j to $O(h^r)$. We observe that

$$\frac{d^{r-1}}{dx^{r-1}}L_j(x;\bar{w})=D_{r-1}=\frac{d^{r-1}}{dx^{r-1}}w(x_j)+O(h^2); \tag{5.10c}$$

this, as (4.3) does in the second-order case, eliminates some of the non-smoothness in the reconstruction eror which is due to the adaptive choice of stencils. Consequently, the ENO scheme based on this reconstruction is rth-order accurate in all L_p norms, including the maximum norm. Note that the correction to the first term in the RHS of (5.10a) takes care of the conservation property (5.2a), i.e.,

$$\frac{1}{h}\int_{I_j}L_j(x;\bar{w})\,dx=\bar{w}_j. \tag{5.10d}$$

Remark. There are other reasonable choices of $L(x; \bar{w})$ and $R(x; \bar{w})$. We may choose

$$L(x; \bar{w}) = \frac{d}{dx} H_r(x; W), \qquad R(x; \bar{w}) = \frac{d}{dx} H_{r+1}(x; W), \tag{5.11}$$

or even

$$L(x; \bar{w}) \equiv R(x; \bar{w}) = \frac{d}{dx} H_r(x; \bar{w}); \tag{5.12}$$

note that the expression for $\hat{g}_{j+1/2}$ in the latter case is much simpler since $d_j(y_1, y_2) \equiv 0$ in (5.7a).

6. Euler Equations of Gas Dynamics

In this section, we describe how to apply the scheme (5.1) to the Euler equations of gas dynamics for a polytropic gas:

$$u_t + f(u)_x = 0 \tag{6.1a}$$

$$u = (\rho, m, E)^{\mathrm{T}} \tag{6.1b}$$

$$f(u) = qu + (0, P, qP)^{\mathrm{T}} \tag{6.1c}$$

$$P = (\gamma - 1)(E - \tfrac{1}{2}\rho q^2). \tag{6.1d}$$

Here ρ, q, P, and E are the density, velocity, pressure, and total energy, respectively; $m = \rho q$ is the momentum and γ is the ratio of specific heats.

The eigenvalues of the Jacobian matrix $A(u) = \partial f / \partial u$ are

$$a_1(u) = q - c, \qquad a_2(u) = q, \qquad a_3(u) = q + c, \tag{6.2a}$$

where $c = (\gamma P/\rho)^{1/2}$ is the sound speed.

The corresponding right-eigenvectors are

$$r_1(u) = \begin{pmatrix} 1 \\ q - c \\ H - qc \end{pmatrix}, \qquad r_2(u) = \begin{pmatrix} 1 \\ q \\ \frac{1}{2}q^2 \end{pmatrix}, \qquad r_3(u) = \begin{pmatrix} 1 \\ q + c \\ H + qc \end{pmatrix}; \tag{6.2b}$$

here

$$H = (E + P)/\rho = c^2/(\gamma - 1) + \tfrac{1}{2}q^2 \tag{6.2c}$$

is the enthalpy.

To compute a left-eigenvector system $\{l_k(u)\}$ which is bi-orthonormal to $\{r_k(u)\}$

in (6.2b), we first form the matrix $\mathbf{T}(u)$, the columns of which are the right-eigenvectors in (6.2b)

$$\mathbf{T}(u) = (r_1(u), r_2(u), r_3(u))$$

and then define $l_k(u)$ to be the kth row in $\mathbf{T}^{-1}(u)$, the inverse of $\mathbf{T}(u)$. We get

$$\begin{aligned} l_1(u) &= \tfrac{1}{2}(b_2 + q/c, \ -b_1 q - 1/c, \ b_1) \\ l_2(u) &= (1 - b_2, \ b_1 q, \ -b_1) \\ l_3(u) &= \tfrac{1}{2}(b_2 - q/c, \ -b_1 q + 1/c, \ b_1), \end{aligned} \tag{6.2d}$$

where

$$b_1 = (\gamma - 1)/c^2 \tag{6.2e}$$

$$b_2 = \tfrac{1}{2} q^2 b_1. \tag{6.2f}$$

Given $\{v_j^n\}$, approximation to $\{\bar{u}(x_j, t_n)\}$, we use (6.2d)–(6.2f) to evaluate the locally defined characteristic variables $\bar{w}_i^k(v_j^n)$,

$$\bar{w}_i^k = l_k(v_j^n) v_i^n \qquad \text{for} \quad i = j - r, \ldots, j + r \quad \text{and} \quad k = 1, 2, 3. \tag{6.3a}$$

Note that j is fixed in (6.3a) while i varies over the points which are relevant to the selection of the stencil for the cell I_j. Thus, the eigenvector system $\{l_k(v_j^n)\}_{k=1}^3$ should be regarded in this context as a constant system of coordinates. Next we apply our scalar algorithm to each of the locally defined characteristic variables in (6.3a); i.e., we select a (possibly different) stencil for each of the characteristic variables and define $R_j(x; \bar{w}^k)$ by (5.9); then we combine these scalar reconstruction by

$$\mathbf{R}_j(x; v^n) = \sum_{k=1}^{3} R_j(x; \bar{w}^k(v_j^n)) r_k(v_j^n). \tag{6.3b}$$

Note that the vector reconstruction (6.3) satisfies all the requirements listed in (1.6).

As in Section 5 we rewrite the rth degree polynomial (6.3b) as a finite Taylor expansion, except that now the coefficients $\{D_k\}$ in (5.9) are vectors. With this convention in mind we proceed to define the vector reconstruction $L_j(x; v^n)$ and the numerical flux $f_{j+1/2}^{\text{ENO}}$ by (5.10) and (5.5), respectively.

We turn now to describe the vector $\hat{g}_{j+1/2}$, which introduced the subcell resolution to the numerical flux (5.1). As we have mentioned earlier in this paper., we use subcell resolution only in the linearly degenerate field ($k = 2$ in (6.2)) in order to improve the resolution of contact discontinuities. We do so by applying the algorithm (5.8) scalarly to the linearly degenerate characteristic field $k = 2$ as follows:

We define

$$\sigma_j = \left| l_2(v_j^n) \frac{d^k}{dx^k} \mathbf{R}_j(x_j; v^n) \right| \qquad \text{for some } k,\ 1 \leqslant k \leqslant r-1, \tag{6.4}$$

$$F_j(x) = \frac{1}{h} \cdot l_2(v_j^n) \left\{ \int_{x_{j-1/2}}^{z} \mathbf{R}_{j-1}(x; v^n)\, dx + \int_{z}^{x_{j+1/2}} \mathbf{R}_{j+1}(x; v^n)\, dx - h v_j^n \right\} \tag{6.5}$$

and, similarly,

$$d_j(y_1, y_2) = \int_{y_1}^{y_2} l_2(v_j^n)[\mathbf{R}_j(x; v^n) - \mathbf{L}_j(x; v^n)]\, dx \tag{6.6a}$$

$$C_{m+1/2}(y_1, y_2) = \int_{y_1}^{y_2} l_2(v_j^n)[\mathbf{R}_{m+1}(x; v^n) - \mathbf{R}_m(x; v^n)]\, dx \quad \text{for } m = j-1, j. \tag{6.6b}$$

The characteristic speed of the linerly degenerate field is the flow velocity q; which can be of different sign in different regions. The definition of $\hat{g}_{j+1/2}$ in (5.8) is formulated as the contribution of the cell I_j to the numerical flux. Therefore, it is convenient to program the calculation of the numerical flux in two stages: First we evaluate

$$\bar{f}_{j+1/2} = \bar{f}_{j+1/2}^{\text{ENO}} \tag{6.7}$$

by (5.5) for all j. Then we sweep over the mesh again and collect the contribution of each cell to the numerical flux. Using FORTRAN conventions this can be described by:

If $q_j^n > 0$ then

$$\bar{f}_{j+1/2} = \bar{f}_{j+1/2} + \frac{1}{\tau} \cdot d_j(x_{j+1/2} - \tau q_j^n, x_{j+1/2}) r_2(v_j^n); \tag{6.8}^+$$

if $q_j^n \leqslant 0$ then

$$\bar{f}_{j-1/2} = \bar{f}_{j-1/2} - \frac{1}{\tau} d_j(x_{j-1/2}, x_{j-1/2} - \tau q_j^n) r_2(v_j^n). \tag{6.8}^-$$

Next we check whether the discontinuity condition

$$\sigma_j > \sigma_{j-1}, \quad \sigma_j \geqslant \sigma_{j+1}, \qquad F_j(x_{j-1/2}) \cdot F_j(x_{j+1/2}) \leqslant 0 \tag{6.9}$$

is satisfied. If one or more of the inequalities in (6.9) is not true, we move on to the next cell. If all the inequalities in (6.9) are true we proceed to calculate as follows:

If $q_j^n > 0$, then

$$\delta_j = \begin{cases} c_{j+1/2}(x_{j+1/2} - \tau q_j^n, x_{j+1/2}) & \text{if } F_j(x_{j+1/2}) \cdot F_j(x_{j+1/2} - \tau q_j^n) > 0 \\ c_{j-1/2}(x_{j-1/2}, x_{j+1/2} - \tau q_j^n) & \text{otherwise} \end{cases} \tag{6.10a}^+$$

and

$$\tilde{f}_{j+1/2} = \bar{f}_{j+1/2} + \delta_j r_2(v_j^n). \tag{6.10b}^+$$

If $q_j^n \leqslant 0$, then

$$\delta_j = \begin{cases} c_{j+1/2}(x_{j-1/2} - \tau q_j^n, x_{j+1/2}) & \text{if } F_j(x_{j+1/2}) \cdot F_j(x_{j-1/2} - \tau q_j^n) > 0 \\ c_{j-1/2}(x_{j-1/2}, x_{j-1/2} - \tau q_j^n) & \text{otherwise} \end{cases} \tag{6.10a}^-$$

and

$$\tilde{f}_{j-1/2} = \bar{f}_{j-1/2} + \delta_j r_2(v_j^n). \tag{6.10b}^-$$

Once we have completed the calculations in (6.10) we move on to the next cell.

7. Numerical Experiments

In this section, we present results of several computer experiments with the ENO schemes (5.5) and their modified version with subcell resolution (5.1); we refer to the latter as ENO/SR. In all these experiments we have used

$$\sigma_j = \left| \frac{d}{dx} R(x_j; v^n) \right| \tag{7.1}$$

and, similarly, $k = 1$ in (6.4) for systems. In all the calculations reported in this section we have used a CFL number of 0.8. The continuous line in Figs. 2–8 represents

We start with the scalar constant coefficient problem

$$u_t + u_x = 0, \qquad u(x, 0) = u_0(x), \qquad -1 \leqslant x \leqslant 1, \tag{7.2}$$

with periodic boundary conditions at $x = \pm 1$. In this case, we take

$$f^R(u_1, u_2) = u_1. \tag{7.3}$$

First, we present numerical experiments with the highly discontinuous initial data

$$u_0(x + 0.5) = \begin{cases} -x \sin(\frac{3}{2}\pi x^2), & -1 < x < -\frac{1}{3} \\ |\sin(2\pi x)| & |x| < \frac{1}{3} \\ 2x - 1 - \sin(3\pi x)/6 & \frac{1}{3} < x < 1. \end{cases} \tag{7.4a}$$

Note that the RHS of (7.4a) is shifted by (-0.5) for purposes of display. We initialized the calculation by taking

$$v_j^0 = \frac{1}{h} \int_{x_j - 1/2}^{x_{j+1/2}} u_0(x)\, dx = \frac{1}{h} [U_0(x_{j+1/2}) - U_0(x_{j-1/2})], \tag{7.4b}$$

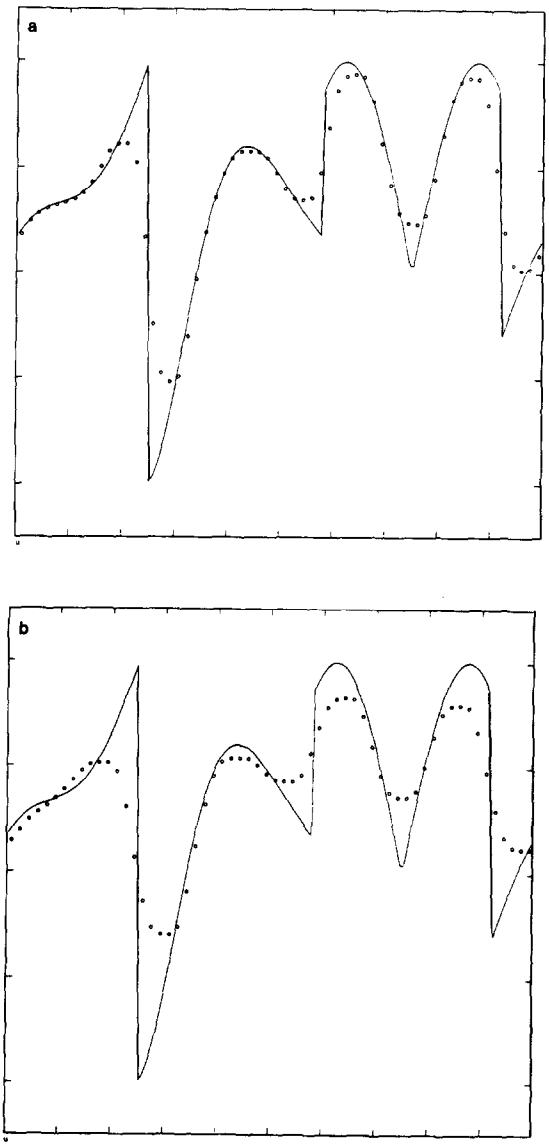

FIG. 2. MUSCL scheme, $-1 \leqslant x \leqslant 1$, $-1.25 \leqslant y \leqslant 1.25$: (a) $t = 2$; (b) $t = 8$.

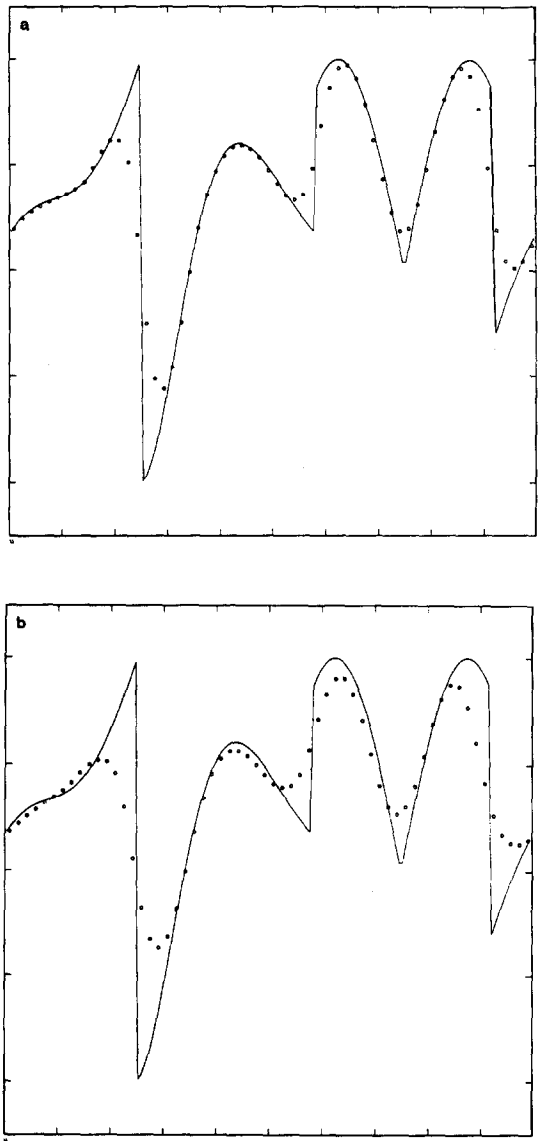

FIG. 3. Second-order ENO scheme, $-1 \leqslant x \leqslant 1$, $-1.25 \leqslant y \leqslant 1.25$: (a) $t = 2$; (b) $t = 8$.

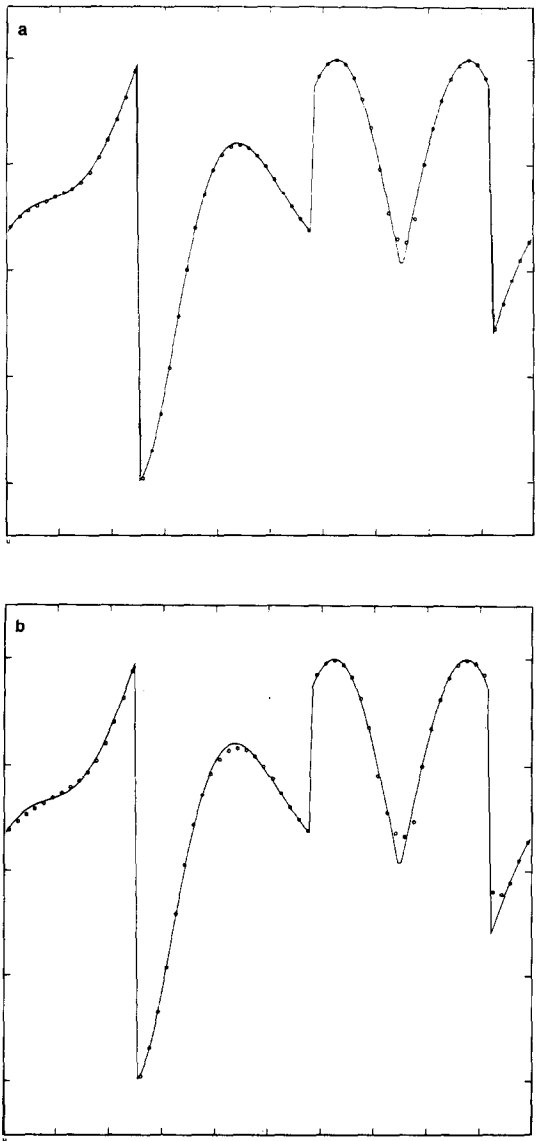

Fig. 4. Second-order ENO/SR, $-1 \leqslant x \leqslant 1$, $-1.25 \leqslant y \leqslant 1.25$: (a) $t = 2$; (b) $t = 8$.

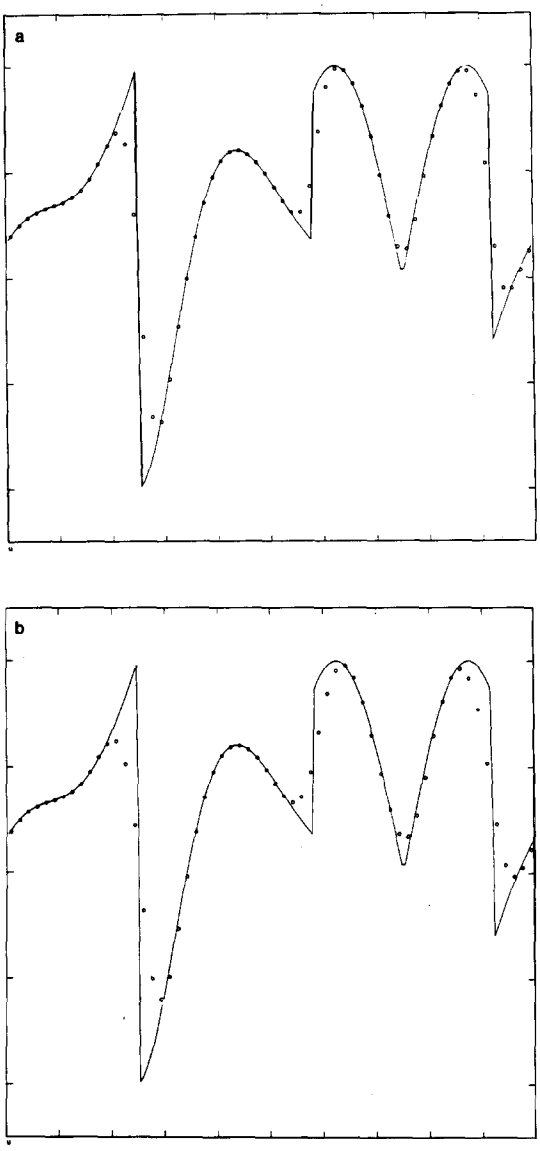

FIG. 5. Fourth-order ENO scheme, $-1 \leqslant x \leqslant 1$, $-1.25 \leqslant y \leqslant 1.25$: (a) $t = 2$; (b) $t = 8$.

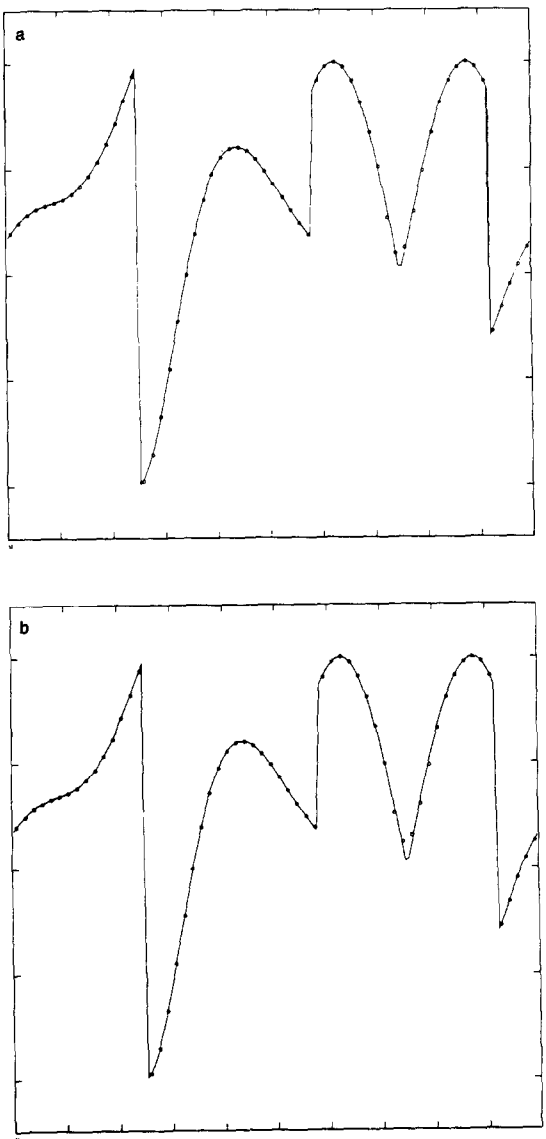

FIG. 6. Fourth-order ENO/SR, $-1 \leqslant x \leqslant 1$, $-1.25 \leqslant y \leqslant 1.25$; (a) $t = 2$; (b) $t = 8$.

where U_0 is the primitive function of $u_0(x)$. In Figs. 2 to 6, we show results with $h = \frac{1}{30}$ (i.e., 60 cells) at: (a) $t = 2$ (after 1 period = 75 time-steps), (b) $t = 8$ (after 4 periods = 300 time-steps). In Fig. 2, we show for sake of comparison the results of the MUSCL-scheme (1.11) with a slope S_j^n defined by

$$S_j^n = m(2(v_{j+1}^n - v_j^n), \tfrac{1}{2}(v_{j+1}^n - v_{j-1}^n), 2(v_j^n - v_{j-1}^n))/h; \tag{7.5a}$$

here $m(x, y, z)$ is the minmod function

$$m(x, y, z) = \begin{cases} s \cdot \min(|x|, |y|, |z|), & \text{if } \operatorname{sgn}(x) = \operatorname{sgn}(y) = \operatorname{sgn}(z) = s \\ 0, & \text{otherwise.} \end{cases} \tag{7.5b}$$

In Fig. 3, we present results of the second-order accurate ENO scheme (4.3), and in Fig. 4 we show results of the corresponding second-order accurate ENO/SR (4.5) with $(4.13)^+$. In Fig. 5, we present the results of the fourth-order accurate ENO scheme (5.5) with $r = 4$, and in Fig. 6 we show the corresponding results of the fourth-order accurate ENO/SR (5.1).

Next we demonstrate the kind of accuracy to be expected from these methods in smooth problems by calculating a refinement sequence for the periodic constant coefficient problem (7.2) with initial data

$$u_0(x) = \sin(\pi x).$$

In Table I, we show the results at $t = 2$ with $h = \frac{1}{4}, \frac{1}{8}, \frac{1}{16}$ (i.e., 8, 16, and 32 cells, respectively). The quantity r_c in this table is the "computational order of accuracy" which is evaluated from two successive calculations by assuming the error to be a constant time h^{r_c}; clearly this definition is meaningful only for h sufficiently small.

TABLE I

Refinement Sequence for $u_t + u_x = 0$, $u(x, 0) = \sin \pi x$ with periodic boundary conditions

	No. of Cells	MUSCL	r_c	2nd Order ENO	r_c	2nd Order ENO/SR	r_c	4th Order ENO	r_c	4th Order ENO/SR	r_c
L_8 error	8	1.454×10^{-1}		6.568×10^{-2}		4.532×10^{-2}		6.674×10^{-3}		8.592×10^{-3}	
			1.52		2.50		1.55		4.90		4.37
	16	5.506×10^{-2}		1.164×10^{-2}		1.546×10^{-2}		2.235×10^{-4}		4.146×10^{-4}	
			1.45		2.19		2.66		4.67		4.32
	32	2.019×10^{-2}		2.556×10^{-3}		2.445×10^{-3}		8.762×10^{-6}		2.082×10^{-5}	
L_1 error	8	7.040×10^{-2}		4.068×10^{-2}		3.098×10^{-2}		4.080×10^{-3}		5.670×10^{-3}	
			1.80		2.42		2.29		4.91		4.80
	16	2.028×10^{-2}		7.600×10^{-3}		6.340×10^{-3}		1.353×10^{-4}		2.042×10^{-4}	
			1.91		2.21		2.84		4.67		4.74
	32	5.380×10^{-3}		1.638×10^{-3}		8.800×10^{-4}		5.300×10^{-6}		7.630×10^{-6}	

Note that in the constant coefficient case the ENO/SR schemes are one-order higher in the L_1-sense than the corresponding ENO schemes.

We turn now to present numerical experiments with the Euler equation of gas dynamics (6.1). In these calculations we take $\gamma = 1.4$ and $f^R(u_1, u_2) = f^{\mathrm{ROE}}(u_1, u_2)$, where we use Roe's linearization [10] to define

$$f^{\mathrm{ROE}}(u_1, u_2) = \frac{1}{2}\left[f(u_1) + f(u_2) - \sum_{k=1}^{3} \delta_k \, |a_k(\hat{u})| \, r_k(\hat{u}) \right], \tag{7.6a}$$

with

$$\delta_k = l_k(\hat{u})(u_2 - u_1); \tag{7.6b}$$

here a_k, l_k, and r_k are the eigenvalues and the left- and right-eigenvectors, respectively. $\hat{u}$ is a particular average of u_1 and u_2 which is defined by:

$$\hat{q} = \langle q\sqrt{\rho} \rangle / \langle \sqrt{\rho} \rangle, \qquad \hat{H} = \langle H\sqrt{\rho} \rangle / \langle \sqrt{\rho} \rangle, \qquad \hat{c} = (\gamma - 1)^{1/2} \sqrt{\hat{H} - 1/2\hat{q}^2}; \tag{7.6c}$$

here $\langle \ \rangle$ denotes arithmetic average, i.e.,

$$\langle b \rangle = \tfrac{1}{2}(b_1 + b_2).$$

In Figs. 7 and 8, we show results of the Riemann initial value problem

$$u_t + f(u)_x = 0, \qquad u(x, 0) = \begin{cases} u_{\mathrm{L}}, & x < 0 \\ u_{\mathrm{R}}, & x > 0 \end{cases} \tag{7.7a}$$

with

$$(\rho_{\mathrm{L}}, q_{\mathrm{L}}, P_{\mathrm{L}}) = (0.445, 0.698, 3.528); \qquad (\rho_{\mathrm{R}}, q_{\mathrm{R}}, P_{\mathrm{R}}) = (0.5, 0, 0.571). \tag{7.7b}$$

These calculations were performed with 100 cells, $h = 0.1$, CFL $= 0.8$, and 85 time-steps. In Fig. 7, we show the density computed by the second-order ENO scheme and in Fig. 8 we show that of the corresponding ENO/SR.

Finally, we present numerical solutions to the problem of two interacting blast waves:

$$u(x, 0) = \begin{cases} u_{\mathrm{L}}, & 0 \leqslant x < 0.1 \\ u_{\mathrm{M}}, & 0.1 \leqslant x < 0.9 \\ u_{\mathrm{R}}, & 0.9 \leqslant x < 1, \end{cases} \tag{7.8a}$$

where

$$\begin{aligned} &\rho_{\mathrm{L}} = \rho_{\mathrm{M}} = \rho_{\mathrm{R}} = 1, \qquad q_{\mathrm{L}} = q_{\mathrm{M}} = q_{\mathrm{R}} = 0, \\ &P_{\mathrm{L}} = 10^3, \qquad P_{\mathrm{M}} = 10^{-2}, \qquad P_{\mathrm{R}} = 10^2; \end{aligned} \tag{7.8b}$$

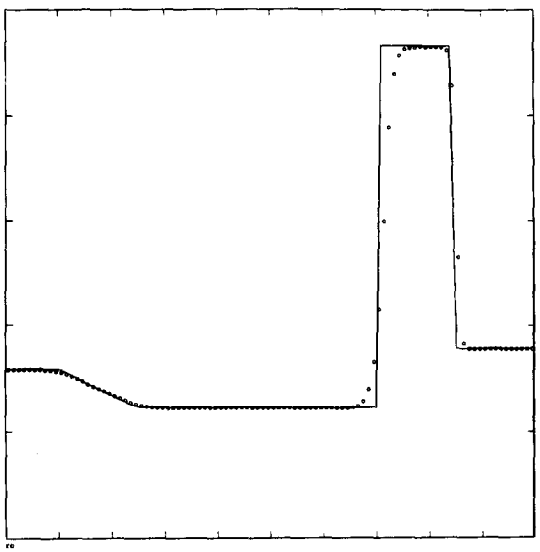

FIG. 7. Second-order ENO scheme, $0 \leqslant x \leqslant 1$, $0 \leqslant y \leqslant 1.4$: Density (85 time-steps).

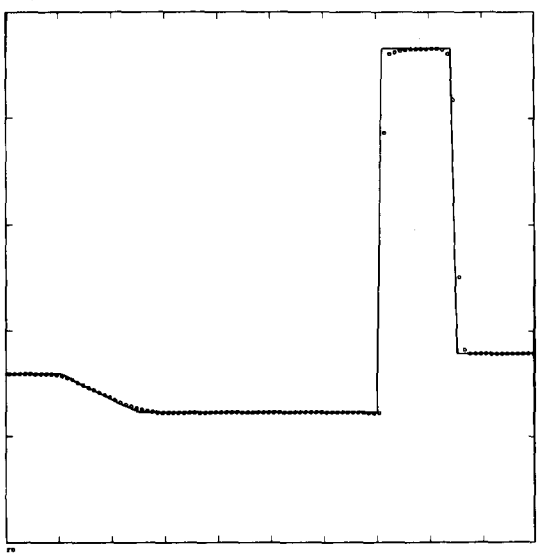

FIG. 8. Second-order ENO/SR, $0 \leqslant x \leqslant 1$, $0 \leqslant y \leqslant 1.4$: Density (85 time-steps).

the boundaries at $x=0$ and $x=1$ are solid walls. This problem was suggested by Woodward and Colella as a test problem; we refer the reader to [11] where a comprehensive comparison of the performance of various schemes for this problem is presented. We refer the reader to [7] for a detailed description of the implementation of the solid wall boundary condition in the ENO schemes.

In Fig. 9, we show the density at $t=0.038$ calculated by the second-order accurate ENO/SR with 800 cells and CFL $=0.8$. The circles in this figure represent values of $R(x_j, \rho^n)$; the continuous line is just the piecewise-linear interpolation of these values. Comparing these results to the solution presented by Woodward and Colella in [11], we find that it shows all the important features of the various interactions and thus can be considered a "converged" solution. We use this piecewise-linear interpolation of the calculation with 800 cells as the "exact solution" in Figs. 10 and 11. The circles in Figs. 10 and 11 are reconstructed values of density in a calculation with 200 cells. In Fig. 10, we show the calculation by the second order accurate ENO scheme; in Fig. 11 we show the results of the corresponding ENO/SR.

In the following, we make several remarks and observations concerning the numerical results presented in this section.

(1) In all our calculations we find that the subcell resolution technique is capable of producing perfctly resolved linear discontinuities. Observe that if $R(x; v^n)$ has a single intermediate value at a discontinuity then this discontinuity is perfectly resolved by $\hat{R}(x; v^n)$.

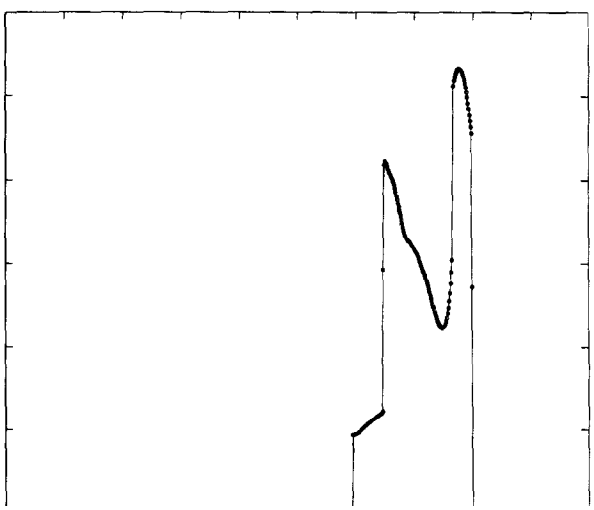

(2) When we study the effect of higher formal order of accuracy in the calculation of discontinuous data by the ENO schemes, we find that the most noticable improvement is due to the reduction in smearing of the linear discontinuitites. However, when we compare the second-order and the fourth-order ENO/SR schemes we see that the improvement is primarily due to higher accuracy in the smooth part of the solution. Consequently, there is no sense in going to higher order when solving a Riemann IVP. To justify the increased computational cost associated with higher order, one needs a lot of structure in the smooth part of the solution.

(3) Comparing the solution of the interacting blast waves (7.8) by the second-order ENO/SR to that of the PPM in [12], we find that the ENO/SR is more accurate. The ENO/SR highly resolves all three contact discontinuities in the problem, while for some reason the PPM well resolves two of the contact discontinuities but smears the one which results from the shock interaction. Another possible explanation for the difference in accuracy may be due to the fact that the ENO/SR is unifomly second-order accurate, while the PPM (because of its monotonicity constraints) reduces to first-order accuracy at points of local extremum.

(4) The numerical results for the Euler equations of gas dynamics clearly demonstrate that shocks are highly resolved by the original ENO schemes, and subcell resolution is not needed there. In any case, the expressions for $\hat{g}_{j+1/2}$ have to be modified before applying subcell resolution to a genuinely nonlinear field, as follows: (i) a_j^n should be replaced by the speed of the shock. (ii) Dissipation proportional to $(a_{j+1/2}-a_{j-1/2})$ should be added to a centered rarefaction wave. Fortunately, if the discontinuity condition (3.9a) is met in the cell I_j, then $\hat{R}(x; v^n)$ is continuous at $x_{j\pm 1/2}$ and no interaction terms need be added to the numerical flux. However, one has to account for the fact that the wave from the interior of I_j crosses its boundaries during the time-step.

APPENDIX: Derivation of the Discontinuity Condition

The reconstruction $R(x; \bar{w})$ is by definition discontinuous at $\{x_{j+1/2}\}$. In regions of smoothness of $w(x)$ the jump of the reconstruction at $x_{j+1/2}$ is of the order $O(h^r)$. When a discontinuity of $w(x)$ is located in the interior of I_j, then the discontinuities of the reconstruction at $x_{j\pm 1/2}$ are fragments of that of $w(x)$. (See Fig. 1b.)

In order to recover a possible discontinuity in the interior of each cell, we would like to associate the reconstruction with the boundaries of the cells $\{x_{j+1/2}\}$, rather than the cells themselves. Let $\tilde{R}_{j+1/2}(x; \bar{w})$ be the polynomial description of such a reconstruction which is valid in the neighborhood of $x_{j+1/2}$. Once this is done we consider reconstructing $w(x)$ in I_j by

$$\hat{R}_j(x; \bar{w}) = \begin{cases} \tilde{R}_{j-1/2}(x; \bar{w}) & \text{for} \quad x_{j-1/2} \leqslant x < \theta_j \\ \tilde{R}_{j+1/2}(x; \bar{w}) & \text{for} \quad \theta_j \leqslant x < x_{j+1/2} \end{cases} \tag{A.1}$$

if possible, i.e., if there is a θ_j such that

$$\tilde{F}_j(\theta_j) = 0, \qquad x_{j-1/2} \leqslant \theta_j < x_{j+1/2}, \tag{A.2a}$$

where

$$\tilde{F}_j(z) = \frac{1}{h}\left\{\int_{x_{j-1/2}}^{z} \tilde{R}_{j-1/2}(x; \bar{w})\, dx + \int_{z}^{x_{j+1/2}} \tilde{R}_{j+1/2}(x; \bar{w})\, dx\right\} - \bar{w}_j. \tag{A.2b}$$

If there is no such θ_j, we define

$$\hat{R}_j(x; \bar{w}) = R_j(x; \bar{w}). \tag{A.3}$$

The only thing which is left open at this point is the definition of $\tilde{R}_{j+1/2}(x; \bar{w})$. It is most natural within the framework of the ENO reconstruction to select the "smoother" of $R_j(x; \bar{w})$ and $R_{j+1}(x; \bar{w})$; i.e.,

$$\tilde{R}_{j+1}(x; \bar{w}) = \begin{cases} R_j(x; \bar{w}) & \text{if } \sigma_j < \sigma_{j+1} \\ R_{j+1}(x; \bar{w}) & \text{if } \sigma_j \geqslant \sigma_{j+1} \end{cases}. \tag{A.4}$$

Here σ_j is a monotone increasing function of the "non-smoothness," such as (3.8a). Note that since $R_i(x; \bar{w})$ is associated with a stencil of points, (A.4) is equivalent to assigning a stencil to $x_{j+1/2}$, the boundary of the cell.

We observe that there is a certain ambiguity in the definition of $\hat{R}_j(x; w)$ in (A.1), since θ_j need not be unique. We remove most of this ambiguity by adopting a policy of "no unnnecessary changes," and agree that

$$\tilde{R}_{j-1/2} = R_j \qquad \text{or} \qquad \tilde{R}_{j+1/2} = R_j \Rightarrow \hat{R}_j = R_j; \tag{A.5}$$

i.e., if one of the candidates for extension into I_j is no smoother than the original R_j, we just retain the original definition in $\hat{R}_j$. From the definition (A.4) of $\tilde{R}$ we can rewrite (A.5) in terms of σ_i as

$$\sigma_j \leqslant \sigma_{j-1} \qquad \text{or} \qquad \sigma_j < \sigma_{j+1} \Rightarrow \hat{R}_j = R_j. \tag{A.5}'$$

Hence we conclude that we define $\hat{R}_j(x; \bar{w})$ to be (A.1) only if

$$\sigma_j > \sigma_{j-1} \qquad \text{and} \qquad \sigma_j \geqslant \sigma_{j+1} \tag{A.6}$$

which is the discontinuity condition (3.8b). In this case $\tilde{R}_{j-1/2} = R_{j-1}$ and $\tilde{R}_{j+1/2} = R_{j+1}$ and the definition (3.9) follows.

REFERENCES

1. P. COLELLA AND P. R. WOODWARD, *J. Comput. Phys.* **54**, 174 (1984).
2. S. K. GODUNOV, *Math. Sb.* **47**, 271 (1959). [Russian]
3. A. HARTEN, *Math. Comput.* **32**, 363 (1978).
4. A. HARTEN, *J. Comput. Phys.* **49**, 357 (1983).
5. A. HARTEN, MRC Technical Symmary Report 2829, University of Wisconsin, 1985 (unpublished).
6. A. HARTEN AND S. OSHER, *SINUM* **24**, 279 (1987); MRC Technical Symmary Report 2823, May 1985 (unpublished).
7. A. HARTEN, B. ENGQUIST, S. OSHER, AND S. R. CHAKRAVARTHY, *J. Comput. Phys.* **71**, 231 (1987); ICASE Report 86–22, April 1986 (unpublished).
8. A. HARTEN, S. OSHER, B. ENGQUIST, AND S. R. CHAKRAVARTHY, *J. Appl. Numer. Math.* **2**, 347 (1986); in *Advances in Numerical and Applied Mathematics*, edited by J. C. South, Jr. and M. Y. Hussaini, ICASE Report 86–18, March 1986.
9. B. VAN LEER, *J. Comput. Phys.* **32**, 101 (1979).
10. P. L. ROE, *J. Comput. Phys.* **43**, 357 (1981).
12. P. WOODWARD AND P. COLELLA, *J. Comput. Phys.* **54**, 115 (1984).